ELSEVIER

Earth and Planetary Science Letters 188 (2001) 421–434

EPSL

www.elsevier.com/locate/epsl

A dynamical investigation of the heat and helium imbalance

Peter E. van Keken [a,*], Chris J. Ballentine [b], Don Porcelli [b]

[a] *Department of Geological Sciences, 425 E University Avenue, 2534 CC Little Building, University of Michigan, Ann Arbor, MI 48109-1063, USA*

[b] *ETH Zürich, Isotopengeologie, NO C 61, Sonneggstr. 5, CH-8092 Zürich, Switzerland*

Received 15 December 2000; received in revised form 26 March 2001; accepted 6 April 2001

Abstract

The terrestrial heat–helium imbalance [O'Nions and Oxburgh, Nature 306 (1983) 429–431] is based on the observation that significantly less ^{4}He is released from the Earth's mantle than is predicted from the radiogenic element budget and observed heat flow. We review recent observations and models of Earth's radioelement distribution and ^{4}He flux and demonstrate that this imbalance remains a robust observation. We explore the hypothesis that the imbalance can be accounted for by different timescales of heat and helium extraction from the mantle system. This is tested using dynamical models of mantle convection that incorporate thermal evolution, helium ingrowth and degassing. The temporal decoupling of heat and helium loss provides large excursions from the mantle heat and helium production ratio and can indeed drop to values as low as those observed. Nevertheless, the duration of these periods is very limited within the 4 Byr model period and the probability that the present-day situation is caused by such an excursion must be considered to be very small. While the average ratio of heat and helium released from the whole mantle convection models is smaller than the production ratio, a significant imbalance remains. An additional mechanism is required to further separate heat from helium.

Keywords: mantle; convection; radioactive isotopes; heat flow; degassing; noble gases

1. Introduction

It is quite clear from differences observed in the isotopic composition of ocean island basalts (OIB) and mid-ocean ridge basalts (MORB) that the mantle system requires the existence of at least two distinct geochemical reservoirs, preserved over long periods of the planet's history. In the past the MORB-source mantle has been assumed to be largely isolated from the OIB-source mantle by the 670 km phase change, with a small degree of material flux to account for radiogenic and noble gas isotope differences between OIBs and MORBs [2–5]. Our understanding of the dynamical and chemical evolution of the terrestrial mantle has undergone an important conceptual change with the clear demonstration of material transfer through the 670 km phase change, both in the form of subducting slabs [6] and in that of plumes originating from the core–mantle boundary [7]. Fluid dynamical simulations of whole

* Corresponding author. Tel.: +1-734-764-1497; Fax: +1-734-763-4690;
E-mail addresses: keken@umich.edu (P. van Keken); ballentine@erdw.ethz.ch (C. Ballentine); porcelli@erdw.ethz.ch (D. Porcelli)

0012-821X/01/$ – see front matter
PII: S0012-821X(01)00343-0

mantle convection that reproduce reasonable surface plate motion and heat flow show that neither the phase changes in the transition zone nor the increase in lower mantle viscosity are able to preserve more than small-scale geochemical heterogeneities that are evenly distributed throughout the mantle system [8,9]. This then presents us with a fundamental problem. What is the nature of the mechanism that provides a well-mixed MORB-source mantle, yet preserves long-lived geochemical heterogeneity deeper in the mantle system? In addressing this problem the relationship between the heat and helium flux at the Earth's surface has been cited as a critical parameter.

The decay of ^{238}U, ^{235}U and ^{232}Th produces both heat and ^{4}He in constant proportions. Based on the radiogenic element heat budget we can predict the amount of heat and helium produced. Assuming both heat and helium are transported with similar efficiencies, we expect a fixed ratio between heat and helium released at the Earth's surface. However, [1] showed that almost an order of magnitude less ^{4}He was degassing from the mantle than would be predicted from this simple relationship. This appears to require a process capable of decoupling heat from helium in the mantle system. In the absence of any obvious mechanism to do this in the shallow mantle, [1] argued that this provided evidence for a deep boundary layer in the mantle through which heat could pass, but behind which ^{4}He was trapped. The boundary layer was assumed to be the 670 km discontinuity.

The development of numerical models of mantle convection to investigate the processes controlling ^{3}He/^{4}He distribution in the mantle requires tracking both ^{4}He ingrowth and degassing as well as the surface heat flux [8,9]. This provides an obvious tool with which to investigate whether the heat–helium imbalance can be accommodated within the constraints of whole mantle convection. The particular advantage of this approach is that these models do not make any assumptions about the relationships between production and loss, and allow us to assess the magnitude of natural variation in heat and ^{4}He flux that occur due to the different mechanisms by which they are extracted from the mantle system. An important modification has been the linkage of heat production and radioelement concentration in the fluid dynamical simulation. This has enabled us to incorporate into the model runs the effect of secular cooling and the higher heat production in the past because of higher radioelement concentrations. In a similar fashion to past work, models incorporate phase changes at 440 and 670 km, and pressure- and temperature-dependent viscosity. Our models reproduce present-day average heat flow with particle surface velocities that are consistent with the rate of present-day plate motion. One of the key questions addressed by this work is whether or not a dynamic simulation of heat and helium in a whole mantle convective regime can create the observed discrepancy between heat and helium. If this is the case, under what circumstances does it occur, and what are the geochemical and geodynamical consequences? Before we address these questions it is useful to assess the robustness of the observed heat and helium imbalance.

2. Production and surface fluxes of heat and helium

The first fundamental constraint on helium and heat comes from the composition of the bulk silicate Earth (BSE). The U content of the Earth is reasonably well known from cosmochemical arguments to be 18.5 ppb [10]. The Th/U ratio of the bulk Earth is known from Pb isotopes systematics to be 3.8 [11]. A value of $K/U = 1.27 \times 10^4$ has been measured for the MORB source mantle [12] and can be applied to the bulk Earth. The total BSE heat production based on these assumptions at present is then 19.2 TW (see [13]), and the production rate of ^{4}He is 829 Mmol/yr. Although there is some controversy regarding the K content of the Earth [14], K supplies only 15% of the heat produced at present. Therefore, the total heat production is relatively insensitive to the K/U ratio. Note that the MORB source is highly depleted in U, Th, and K, and it is logical to assume that the mantle inventory of these elements resides somewhere below this depth.

As we are mostly interested in the mantle con-

tribution to heat and helium, it is important to consider the role of the concentration of incompatible elements in the continental crust. A large fraction of the Earth's U, Th, and K, estimated between 24% [15] and about 50% (see references in [16]), is presently in the continental crust. It can be assumed that the helium flux out of the crust is equal to that of production within the crust [1]. Studies of the accumulation of ^{4}He in regional aquifer systems [17–19] have come to the same conclusion. Similarly, it is generally assumed that heat production in the crust is equal to the flux of crustal heat out; calculation of the U content of the crust is often based upon this assumption (e.g., [15]). Therefore, the issue of the separation of heat from helium centers only on the mantle fluxes. We can estimate the mantle production of heat and helium by subtracting the amount of production in the continental crust, which leads to a reduction of 24–50%. In our calculations we will assume a crustal heat production of 6 TW (30% of the 19.2 TW BSE heat production). This leaves a mantle heat production of 13.2 TW.

We can now compare the predicted mantle fluxes with those observed. A global investigation of the Earth's heat loss yields a present-day heat flow of 44 TW [20]. To obtain the mantle heat flow we must subtract the contributions from the crust and the core. Constraints based on thermal core cooling histories and driving mechanisms for the geodynamo provide estimates for core heat loss of 3–7 TW [21,22]. Subtracting further the crustal heat production of 6 TW we find a mantle heat loss of 31–35 TW. In the mantle, 13.2 TW can be attributed to present-day mantle heat production, leaving the remainder (17–22 TW) to be attributed to secular cooling of the mantle. Assuming a mantle heat capacity of 1250 J/kg K and mass of 4×10^{24} kg, this translates to a secular cooling rate of 110–130 K per Byr, which is much larger than what can be inferred for the change in upper mantle temperature from surface geology [23]. A possible solution to this problem is to assume that heat production is concentrated in the deeper interior and that the heat transport from this deeper interior is inefficient.

The contrast between predictions and observations is significantly larger when considering the helium fluxes. The largest and most clearly defined mantle helium flux is from mid-ocean ridges. There, the flux of ^{3}He into sea water has been estimated to be 1000 ± 250 mol/yr based on helium saturation anomalies in sea water and sea water advection rates [24,25]. This value represents an average over the last 1000 years. Using an average value of $^3\mathrm{He}/^4\mathrm{He} = 8R_a = 1.1\times10^{-5}$ results in a ^{4}He loss of 89 Mmol/yr.

The flux of mantle-derived helium through the continental crust by transport into the lower crust has been estimated by [19] to be less than 3×10^7 atoms/m^2 s in stable regions and 4×10^9 atoms/m^2 s in extensional areas based on a study of the Pannonian Basin. Note these are based on limited hydrogeological studies and integrate fluxes over short timescales. Using an area of 2×10^{14} m^2 for continents and margins and assuming 10% is under extension, this yields a total ^{4}He flux of 4.3 Mmol/yr [19]. While there is some uncertainty in this number, this flux appears to be much lower than that at ridges. The amount of volcanism at subduction zones has been estimated from [26] to be 1.0 km^3/yr based on data from a range of island arcs. This is consistent with estimates of crustal growth [27]. If it is assumed that 1 km^3/yr is generated by 10% melting of upper mantle (with a MORB helium isotopic signature), then the flux is 5% of that of MORB. Consideration of melting of other subducted components that do not contain mantle helium reduces this.

The helium flux at intraplate volcanism can be calculated from the rate of magma production and average ^{4}He concentration. Estimates of the rate of magma production are $0.4–7\times10^{15}$ g/yr [26,28–30]. This is less than 11% of the mid-oceanic ridge production rate of 6.3×10^{16} g/yr [31]. Since the source regions of the OIB volcanics have $^3\mathrm{He}/^4\mathrm{He}$ ratios higher than that of MORB, the He concentration may also differ. Measurements of He and CO_2 in Hawaiian basalts have been used to obtain $1.4–4.2\times10^{13}$ atoms/g [32]. Vent measurements of He/CO_2 and flux estimates give 4.2×10^{13} atoms/g [33]. Using the highest ratio and largest magma generation rate yields a flux of 0.5 Mmol/yr. In the context of layered mantle

Table 1
Helium flux from the upper mantle

Source	^{4}He flux (Mmol/yr)
Oceanic crust formation	89
Basins in continents	4.3
Hot spots	0.5
Subduction zones	4.5
Total	98.3

models that predict lower and upper mantle values of 1.5×10^{15} and 7.2×10^{13} atoms/g respectively (e.g., [4,5]), these values have been interpreted as representing those of recently degassed magmas. However, hotspot materials exhibit a wide range of ^{3}He/^{4}He ratios that indicate an average contribution by mass of material containing high ^{3}He/^{4}He that is relatively small. It has been estimated that plumes contain about 10% of material from below the boundary layer they originate from [3,34]. Assuming 10% melting of a mixture of 90% upper mantle material and 10% high ^{3}He/^{4}He lower mantle material with the model-derived concentrations produces up to 83 Mmol/yr, which is close to the flux at mid-ocean ridges. However, this is based on a layered mantle model, contrary to the modelling assumptions made here. The He fluxes are summarized in Table 1. Neglecting the higher model-dependent hot spot flux the observed total flux is 98.3 Mmol/yr, which is about 6 times less than the 580 Mmol/yr produced in the mantle. This new check on the robustness of the heat–helium imbalance clearly indicates that a significant discrepancy exists.

3. Model formulation and numerical approach

In this paper we solve the equations governing convection in the Earth's mantle, assuming that the mantle can be described as an anelastic and weakly compressible fluid at infinite Prandtl number. Assuming the extended Boussinesq approach, and variable thermal diffusivity and expansivity, we can write the equations of motion as:

$$-\nabla P+\nabla\cdot(\eta\dot{\varepsilon})=Ra\alpha\rho T\hat{\mathbf{g}} \tag{1}$$

and the mass conservation equation as:

$$\nabla\cdot\mathbf{v}=0 \tag{2}$$

The heat equation incorporates terms that describe viscous heating and adiabatic cooling and heating, and can be written as:

$$\frac{\partial T}{\partial t}+(\mathbf{v}\cdot\nabla)T+\alpha Diw T=$$

$$\nabla\cdot(\kappa\nabla T)+Q+\frac{Di}{Ra}\sigma_{ij}\frac{\partial u_i}{\partial x_j}-\alpha Diw T_0 \tag{3}$$

(e.g., [35]). The equations above are non-dimensional. The symbols representing physical quanti-

Table 2
Dimensionless quantities

Symbol	Quantity	Non-dimensionalization
P	dynamic pressure	$h^2/\eta_0\kappa_0$
η	dynamic viscosity	η_0
$\dot{\varepsilon}$	deviatoric strain rate tensor	h^2/κ_0
α	thermal expansivity	α_0
ρ	density	ρ_0
T	temperature	ΔT_0
$\hat{\mathbf{g}}$	unit vector in the direction of gravity	g
$\mathbf{v}$	velocity vector	h/κ_0
w	upward velocity component	h/κ_0
t	time	h^2/κ_0
κ	thermal diffusivity	κ_0
Q	volumetric radiogenic heating	$h^2/c_p\kappa_0\Delta T_0\rho_0$
T_0	surface temperature	ΔT_0

Table 3
Dimensional constants

Symbol	Quantity	Value
ρ_0	reference mantle density	4500 kg m^{-3}
g	gravitational acceleration	9.8 m s^{-2}
α_0	surface thermal expansivity	3×10^{-5} K^{-1}
κ_0	average thermal diffusivity	10^{-6} m^2 s^{-1}
ΔT_0	temperature contrast across mantle	3000 K
h	depth of the mantle	2885 km
η_0	reference mantle viscosity	10^{22} Pa s
c_p	mantle specific heat	1250 J K^{-1} kg^{-1}

ties and their non-dimensionalization is explained in Table 2.

The Rayleigh number Ra and dissipation number Di are given by:

$$Ra = \frac{\rho_0 g \alpha_0 \Delta T h^3}{\eta_0 \kappa_0} \tag{4}$$

and:

$$Di = \frac{\alpha_0 g h}{c_p} \tag{5}$$

The quantities on the right hand sides are dimensional and are explained in Table 3.

We solve the equations in a 2D cylindrical geometry where we have rescaled the radii of the core and the mantle such that we have a better approximation for the curvature of the spherical Earth [36,37]. The non-dimensional radii of this model are inner radius $R_1 = 0.4292$ and outer radius $R_2 = 1.4292$ which guarantees that the ratio of mantle and core surface area is the same as that in the spherical Earth. The rescaled cylindrical models provide much better similarity to the heat and mass transport properties of the spherical Earth. This is of particular importance for models that include secular cooling and radiogenic heat production, as the incorrect volume and surface predictions cause errors in the modeling of the thermal evolution of the Earth [37].

We assume depth-dependent thermal diffusivity and expansivity, using the relations:

$$\alpha(z) = \rho(z)^{-2} \tag{6}$$

and:

$$\kappa(z) = \rho(z)^3 / \langle \rho \rangle \tag{7}$$

where the density is given by:

$$\rho(z) = e^{Diz} \tag{8}$$

and z is the non-dimensional depth, normalized by the depth of the mantle. We will use $Di = 0.2$. We apply the further approximation that $\rho = 1$ in the right hand side of Eq. 1.

We use time-varying radiogenic heat production, based on the best estimates for present-day BSE concentrations ([13]; Table 4). For simplicity, we ignore the extraction of radioelements by crust formation, and assume that the radioelements are distributed in a uniform manner through the mantle. Our simulations are started from a previous time-dependent model run where we assumed constant heat production at the level of 4 Byr ago, and a fixed core–mantle boundary temperature of 3273 K. Using this as initial condition we compute the evolution of the model over 4 Byr. During the simulation the temperature of the core is updated using a simple cooling expression based on the core heat flow:

$$\rho_c c_c V_c \frac{dT_c}{dt} = -q_c S_c \tag{9}$$

Table 4
Radiogenic decay constants

Isotope	Decay rate (1/Byr)	Present-day concentration (ppb)	Heat production (W/kg)
^{238}U	0.155	20.1	9.47×10^{-5}
^{235}U	0.985	0.143	5.69×10^{-4}
^{232}Th	0.0495	76.4	2.63×10^{-5}
^{40}K	0.554	28.0	2.95×10^{-5}

where S_c is the surface area of the core, V_c is the volume of the core, T_c is the core temperature (which is assumed to be identical to the temperature at the core mantle boundary), $\rho_c = 11\,000$ kg m^{-3} is the average density of the core, and $c_c = 500$ J/kg K is the average core specific heat.

We use a moderately temperature- and pressure-dependent viscosity which is written in non-dimensional form as:

$$\eta(T,p) = \eta_0(z)\exp\left(\frac{A}{T_0+T}\right) \quad (10)$$

where $A = A_0$ in the upper mantle and $A = A_0(1+A_1(z-z_{670})/(1-z_{670}))$ in the lower mantle. z_{670} is the non-dimensional depth of the 670 km discontinuity, T_0 is the non-dimensional surface temperature (273 K), and A_0 and A_1 are constants that determine the temperature and pressure dependence of viscosity. See [38] for more details. The pre-factor η_0 is chosen such that the non-dimensional viscosity at $z = 0$ is equal to 1. We also impose a stepwise increase of this pre-factor by a factor of 10 in the lower mantle. The effects of the 400 and 670 km phase changes are taken into account [8,9].

We monitor degassing in a manner similar to that in [8,9]. We impose a number of degassing zones (100 km deep by 100 km wide) at the surface and distribute about 103 000 tracers in the model (which corresponds to an average distance of 20 km between neighboring tracers). These tracers initially contain the BSE values of U, Th and K at 4 Byr ago. Unlike ^{4}He, which is lost to space, ^{40}Ar accumulates in the atmosphere and provides an important test of the efficiency of mantle outgassing. In addition to ^{4}He ingrowth [8] we also follow the ingrowth of ^{40}Ar which is given at each time step Δt:

$$\Delta[^{40}\mathrm{Ar}] = r[^{40}\mathrm{K}](1-\mathrm{e}^{-\lambda_{40}\Delta t}) \quad (11)$$

Here $\lambda_{40} = 0.554$/Byr is the decay time for ^{40}K and $r = 0.10$ is the relative amount of ^{40}K that decays into ^{40}Ar. At each time step we calculate the amount of degassing of ^{3}He, ^{4}He and ^{40}Ar by extracting 90% of the gases from those particles that are in a degassing zone.

Eqs. 1–3 are solved using a finite element approach based on the general tool box Sepran [39]. The Stokes equations (Eq. 1) and incompressibility constraint (Eq. 2) are solved using a penalty function approach. The time-dependent heat equation is solved using a second order predictor-corrector method after Petrov–Galerkin discretization [40]. The tracers are advanced using a fourth order Runge–Kutta method. The time step is limited to 50% of the Courant–Friedrichs–Levy criterion. The numerical implementation has been extensively tested against standard mantle convection benchmarks [41,42] as well as published results by other workers [37].

4. Results

Fig. 1 shows a snapshot of the temperature field (after 4 Byr) and depth profiles of average viscosity and temperature at 1 Byr intervals. The surface-based Rayleigh number is 3×10^5, which is lower than the volume-averaged Rayleigh number (mostly due to the strong reduction of viscosity in the upper and part of the lower mantle). The temperature snapshot provides a typical view of the model simulations performed here. The principal features are qualitatively similar to those in the models of [9]. The influence of both the viscosity increase in the lower mantle and the endothermic character of the 670 km discontinuity causes downwellings to be retarded at the top of the lower mantle. The phase change is not strong enough to prohibit flow through this boundary and a variety of interactions with the boundary are visible. These range from thickening upon penetration (at 1 o'clock), draping upon the phase boundary (at 10 o'clock) or temporary blocking (at 2 and 7 o'clock). The 'horseshoe' patterns that are visible at the tip of downwellings that have just penetrated into the lower mantle are caused by this tendency of the phase boundary to temporarily block the penetration, causing symmetric broadening of the downwelling at the boundary. Upwellings at the base of the mantle are rather slow and broad, which is caused by a combination of the low amount of heat flowing from the

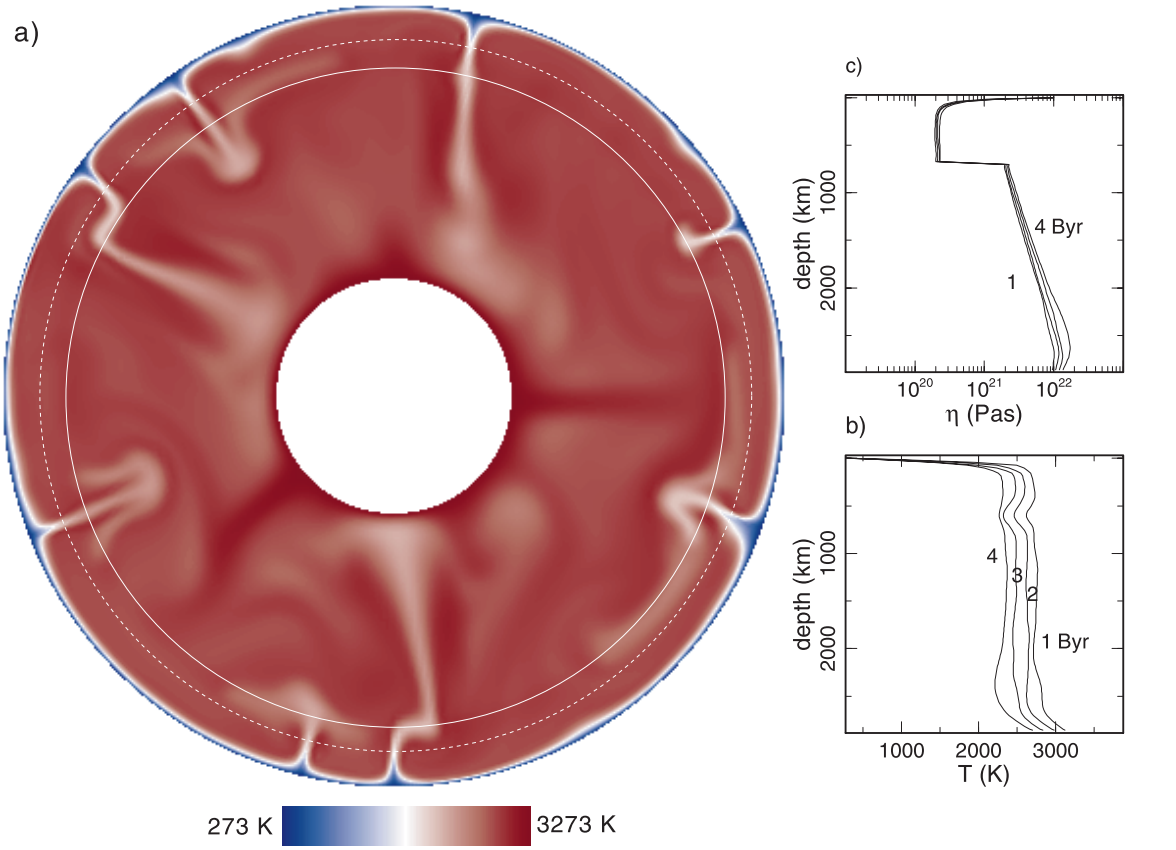

Fig. 1. (a) Snapshot at 4 Byr of compressible mantle convection model with phase transitions and temperature- and pressure-dependent rheology. $Ra = 3 \times 10^5$. (b) Radially averaged temperature profile at 1 Byr time intervals. (c) Radially averaged viscosity profiles at 1 Byr time intervals.

core, the high viscosity, low expansivity and high thermal diffusivity.

In the viscosity formulation we used used $A_0 = 0.2$ and $A_1 = 0.9826$. This provides a viscosity profile that looks similar in the sublithospheric mantle to that obtained from geodetic inversions [43]. The viscosity is only moderately temperature-dependent to avoid the lithosphere from acting as a rigid lid. As a consequence, the downwellings are weaker than what we expect for Earth-like slabs, and the effect of secular cooling on viscosity is not as dramatic as we can expect if the Earth were dominated by the high activation energy of, say, an olivine rheology.

Using the model shown in Fig. 1 as base model we ran a number of simulations with increasing Rayleigh number. We used both the full cylinder geometry shown in Fig. 1 and a half cylinder geometry. We tested explicitly whether this geometry reduction had an influence on the convection and mixing behavior, but we found no essential differences with regard to heat loss and degassing properties.

The choice of the number of degassing zones is based on the relative degassing efficiency of the cylindrical model compared to that of the present-day Earth. Assuming a present-day MORB generation of 20 km^3/yr and 10% melting we can estimate that 200 km^3/yr of mantle is affected by degassing. At this rate it takes approximately 4.5 Byr for the mass of the mantle to be processed. For the cylindrical model we process (assuming an average speed of 5 cm/yr and a 100 km wide degassing zone) an area of 0.005

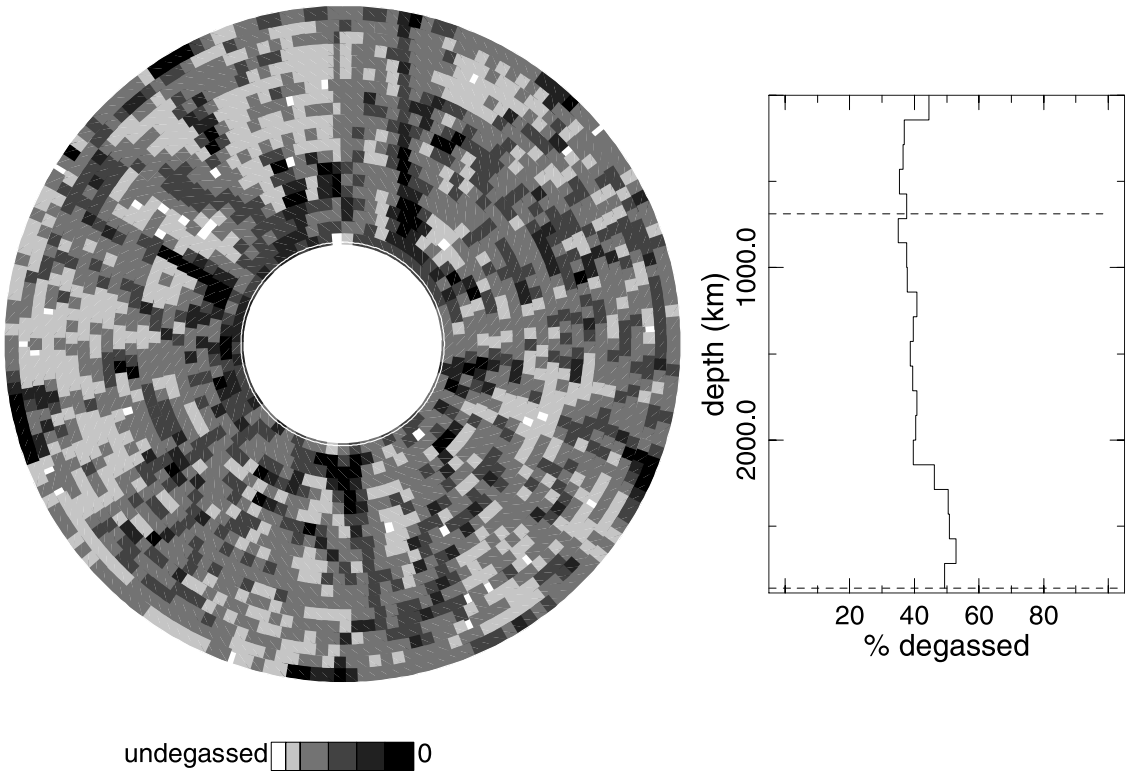

Fig. 2. Example of effects of mantle degassing over 4 Byr for the model shown in Fig. 1. Black indicates strongly degassed mantle.

km^2/yr per degassing zone. The total cylindrical area is 80×10^6 km^2 so it would take 1.6×10^{10} yr to process the entire mantle through one degassing zone. Thus 3.6 degassing zones are required to meet the degassing efficiency of the present day-spherical Earth. However, we can also expect that the degassing efficiency was higher in the past. The cases with the larger number of degassing zones mimic such an evolution by imposing an average degassing rate that is somewhat higher than present-day. Although we incorporate the effects of secular cooling and higher radiogenic heat production in the past, our viscosity law most likely underestimates the effects of the higher temperatures on convective speeds. Because it is unknown how degassing took place in the past, we will use the number of degassing zones as a free parameter. We will use between three and six degassing zones for the full cylinder geometry in order to test the model sensitivity to this parameter. We will use the amount of ^{40}Ar degassed as a tentative test for the applicability of each model.

Fig. 2 shows the degassing of ^{3}He after 4 Byr for the model shown in Fig. 1. We binned the particles using a similar grid as used in [8,9]. White indicates undegassed mantle, whereas black represents fully degassed mantle. The radially averaged amount of ^{3}He is shown on the right. In this model we used five degassing zones, but due to the relatively low Rayleigh number the amount of degassing after 4 Byr is less than what we expect for the Earth. The amount of ^{40}Ar degassed in this model is just 30%, which is well below the observed value of 50%. Note that even though the phase transition and viscosity increase at 670 km depth have a strong influence on the flow geometry, there is no preservation of large-scale heterogeneity. Small-scale heterogeneity (e.g., slab features) can be preserved for several hundreds of millions of years. There is a minor

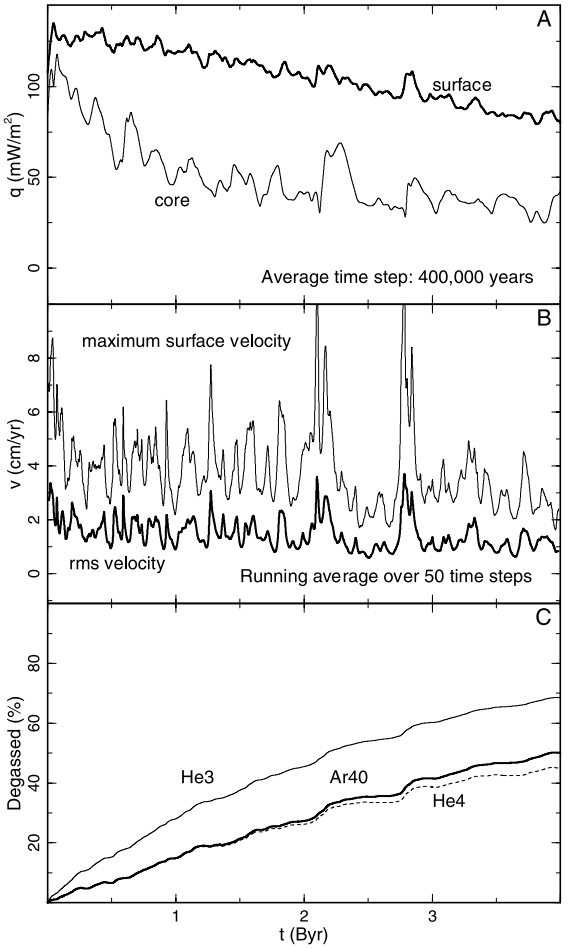

Fig. 3. Evolution of heat and mass transport characteristics. (A) Surface and core heat flow. (B) Maximum surface velocity and rms mantle velocity. (C) Relative amount of degassing as function of initial amount (^{3}He) or amount produced by radiogenic decay (^{40}Ar, ^{4}He).

tendency for degassed downwellings to accumulate near the base of the mantle, due to the sluggishness of convection there. The simultaneously computed evolution of ^{3}He/^{4}He provides an estimate of the model heterogeneity that can be compared to observed mantle heterogeneity. For the model shown in Fig. 2 we find a variance of approx. 10% in the uppermost mantle (top three rows of bins) which is in good agreement with the observed variation of ^{3}He/^{4}He = 8.18 ± 0.73 R_a [44].

The evolution of heat flow, surface velocity and degassing for a model at higher surface Rayleigh number ($Ra = 10^6$) is displayed in Fig. 3. In this case we used a half cylinder geometry and three degassing zones. This would correspond to six degassing zones in the full cylinder geometry and is consequently the model that has the highest rate of degassing. Fig. 3A shows the surface and core heat flow. Although the calculations are performed using non-dimensional variables, we have rescaled these to dimensional values, using the reference values in Table 3 and taking into account the depth variations in thermodynamical parameters. A model run takes approximately 10 000 time steps, so that a typical time step is 400 000 years. The model is characterized by gradual cooling. Our primary test of each model was

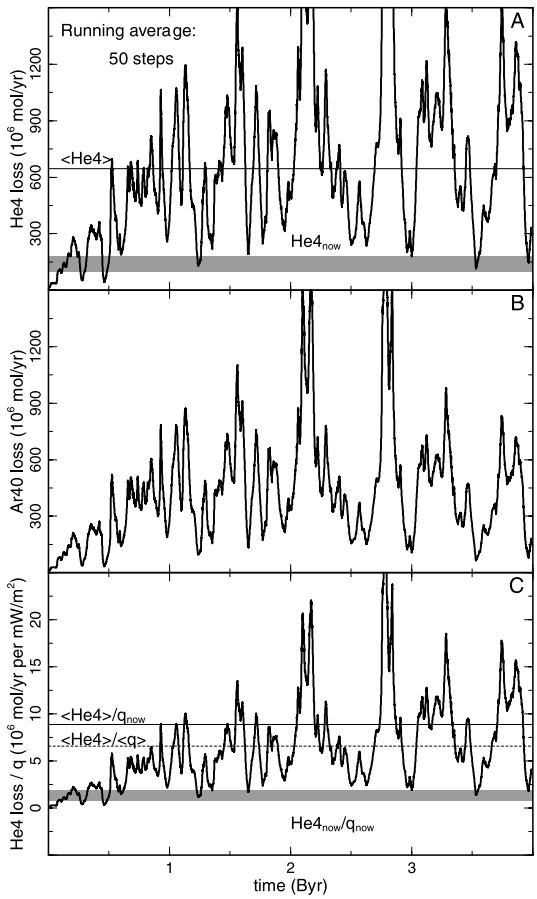

Fig. 4. Degassing rates (20 Myr running average) of: (A) ^{4}He; (B) ^{40}Ar. (C) ^{4}He as a function of heat loss.

the correspondence of the surface heat flow after 4 Byr with that of the present-day Earth. For this we use the present-day heat loss of 44 TW [20] minus the crustal contribution (6 TW), which corresponds to 73 mW/m^2. All models presented here satisfy this criterion within a reasonable range (10%).

Due to the moderate temperature dependence of viscosity the maximum surface velocity and the rms velocity (Fig. 3B) do not change dramatically during the secular evolution. For graphical output reasons we display the running average over 50 time steps (20 Myr).

The time-integrated degassing of ^{3}He (relative to initial mantle value), ^{4}He and ^{40}Ar (both relative to the amount produced by radioactive decay) is shown in Fig. 3C. The amount of ^{40}Ar released compares well with the present-day amount in the atmosphere.

Fig. 4A plots the amount of ^{4}He released as a function of time. The mean value $\langle^4\mathrm{He}\rangle$ (averaged over 4 Byr and indicated by the top horizontal line) is 660×10^6 mol/yr. This is a significant amount below the present-day production of 870×10^6 mol/yr and is largely due to the inefficiency of degassing. The gray bar indicates the range of observed values of ^{4}He (Table 1). Note that there are large excursions from the mean value, even after applying the 20 Myr running average. The model shows occasional excursions that are within the present-day range. This illustrates very clearly the importance of considering time dependence in arguments regarding the heat–helium imbalance. It is logical that the rate of ^{40}Ar loss mimics the ^{4}He loss with minor differences due to the different decay times (Fig. 4B).

The variations in helium loss overwhelm those of the heat loss and as a consequence the graph of heat vs. helium (Fig. 4C) mimics that of helium loss (Fig. 4A). Horizontal lines are plotted that indicate the ratios of (i) time-averaged helium loss over present-day heat loss; (ii) time-average helium loss over time-averaged heat loss; (iii) present-day helium loss over present-day heat loss.

A summary of the results of six model runs is displayed in Fig. 5. We explored three different Rayleigh numbers and used two different sets of

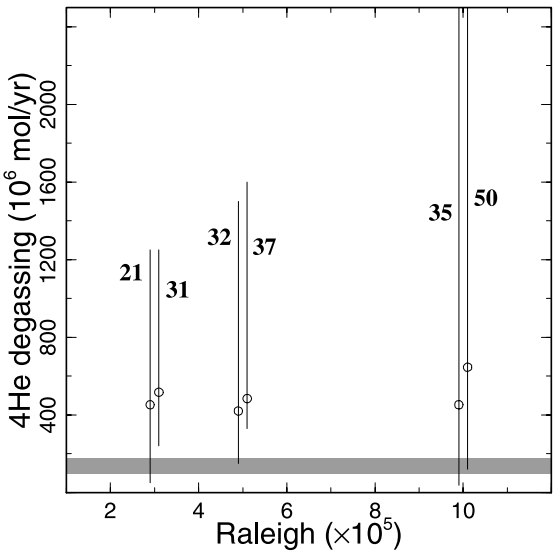

Fig. 5. Summary of the four degassing flux in the six model simulations used in this paper. For three different surface Rayleigh numbers we used between three and six degassing zones. The circles show the average flux and the lines indicate the maximum and minimum values after applying a 20 Myr running average. The numbers near the circles identify the percentage of radiogenic Ar that is degassed in each simulation.

degassing zones. For each Rayleigh number there are two results: the one on the left corresponds to the one with the lowest number of degassing zones. The circles indicate the average degassing rate and the vertical bar indicates the range of degassing rates (after applying the 20 Myr running average). The bold numbers indicate the percentage of ^{40}Ar degassed after 4 Byr. The gray bar indicates the range for present-day loss. There are several trends visible. In general the average degassing rate increases with Rayleigh number (although weakly) and with number of degassing zones (more strongly). The range of degassing rates increases strongly with Rayleigh number. All simulations show excursions to low degassing rates that are below or near the present-day value.

5. Discussion

The models presented here provide a simple test

of the hypothesis that the different timescales of heat and He loss from an otherwise uniform Earth can explain the observed separation of terrestrial heat and helium loss. The mechanism of heat loss within the models is across a uniform temperature boundary layer at the surface, while the helium loss is by degassing at localized ridge analogues. The immediate effect of these different extraction processes illustrates that decoupling of the heat and helium flux does occur on a timescale that results in significant constructive or destructive interference of the He fluxes. Nevertheless, the resulting variance of the heat/He, modulated by a 20 Myr running average, only very occasionally drops as low as the present observed value (Fig. 4). Although this is a tentative explanation for the heat–helium imbalance, we do not consider this likely on statistical grounds. It is important to recognize that the frequency and length of the excursions is dependent on a number of model assumptions, which include the length of the running average employed, the model time step and the spatial distribution of the degassing zones. A much more detailed investigation of the influence of these discrete quantities would be necessary if one wishes to assume that we are currently in one of these large excursions from the mean. This would also require that the mantle approaches the model He concentrations, which are approximately four times higher than current estimates for the MORB source. Average degassing flux over 4 Byr would then have to be four times higher than present-day, with a possible maximum amplitude of up to eight times present-day. The residence time of He in both the oceans and atmosphere is small compared to the time resolution of the model and any record of higher degassing rates in these reservoirs may simply have been lost. Determination of the mantle noble gas concentration independent of the ^{3}He flux is not currently available, but would provide a critical test for any extreme deviation from mean behavior.

The Earth has cooled with time [21,23], demonstrating that heat is being lost faster than it is being produced within the Earth. In the case of ^{4}He, the present-day amount produced in the mantle is 830 Mmol/yr. This contrasts with the present-day flux of 102–185 Mmol/yr and suggests that unlike heat, helium is produced within the mantle faster than it can escape, and is therefore increasing in concentration. The models of whole mantle convection presented are also increasing in ^{4}He concentration, losing on average only 660 Mmol/yr, compared to the 4 Byr average production in the BSE mantle of 1470 Mmol/yr. This result demonstrates that these models do not reach a steady state with respect to helium production and loss within the 4 Byr run time.

An underlying dynamical assumption is that we use models with secular cooling that evolve to a present-day state with similar heat flow and plate velocities as the Earth. It is not clear how the convective vigor of the Earth has changed during its evolution. However, an important upper limit to the Earth's convective vigor as measured by degassing is that 50% of the radiogenic Ar is now in the atmosphere. All our models satisfy this constraint. The rheological law that we employ is less dependent on temperature than that of typical mantle silicates and we therefore expect to underpredict the sensitivity of dynamics to changes in global temperature. To test how this influences our results we have studied the evolution of models for a range of Rayleigh numbers and numbers of degassing zones. Increasing either parameter increases the convective vigor. As shown in the summary diagram (Fig. 5) the principal observations hold for the range of parameters that we investigated.

Our model approach does not take into consideration the extraction of radioelements into the crust. This model simplification results in higher internal heating within the shallow regions of the mantle than in the radioelement-depleted MORB-source mantle. However, previous models show that uniform radioelement concentration plays only a minor role in determining convective vigor [9]. It should be noted that if much of the K in the mantle is extracted by early crust formation (e.g., [27]) then the amount of ^{40}Ar degassed over time from the mantle may be less than the 50% targeted by our model runs.

The main conclusion we draw is that the heat–helium imbalance cannot be solved by differential near-surface extraction of heat and He in the con-

text of a whole mantle convective regime. In this respect we have to consider what type of process or system can be responsible for this. A boundary that allows diffusive loss of heat while retaining He provides a potential solution [1] and has the added attraction of providing a region of the mantle into which the missing radioelements can be stored. It also provides a long-lived geochemical reservoir capable of producing the time-evolved radiogenic isotopes found in OIB systems [45]. The shape and size of such a reservoir, as well as the mechanisms of creation and preservation, are part of an ongoing and as yet unresolved debate. Although such a boundary layer has been assumed in the past to exist at the 670 km discontinuity, high resolution seismic tomography quite clearly shows significant mass transfer across this boundary both in the form of slabs and in that of plumes [6,7]. Furthermore, the effects of phase changes and a high viscosity lower mantle alone are clearly not enough to prevent mixing across the whole mantle system [8,9].

Alternative boundaries include the 'hot abyssal layer' model of [46] which is a variation on the classical layered model where the interface has been pushed deeper into the lower mantle. It shares with it some of the strengths and weaknesses. Unresolved problems with this model include the potential overheating and blanketing of the core due to the high concentration of radionuclides [47]. A fundamental assumption is that the interface is irregular and ill-defined, such that it can escape seismological detection. Some dynamical examples of the feasibility of high amplitude topography have been provided by [46], but these were in models with relatively low convective vigor. At vigor approaching that of the present-day Earth it is predicted that the interface becomes mostly smooth and sharp and should be visible by traditional techniques [48].

The 'blob' model of [49] avoids these problems of overheating and seismological detection by assuming that the compositional heterogeneity is preserved in isolated blobs that due to their high viscosity escape mixing with the rest of the mantle. The high surface to volume ratio of the blobs compared to a layer keeps the blobs relatively cool. However, a dynamic mechanism that keeps the blobs separated and suspended in the mantle has not yet been fully demonstrated.

A third model introduces chemical heterogeneity by plate tectonic recycling of oceanic crust and harzburgitic mantle [50]. In this model it is assumed that the crust and harzburgite form an enriched layer at the base of the mantle. Although the model seems to satisfy a number of constraints from isotope geochemistry, it is not clear that it can be the reservoir for the missing BSE radionuclides. The volume of the proposed reservoir is quite small and the required high U, Th, K concentrations would readily overheat this layer. Nevertheless, this model is attractive because it creates and preserves heterogeneity through known physical mechanisms and could well be a partial answer to the problem of the missing heat and helium in the Earth's mantle.

In order to make further progress in this matter it is essential to address the mass and heat balance, in addition to investigating the dynamical feasibility of proposed mechanisms. A study such as that presented here provides such a crucial test. In future studies we expect to be able to address dynamical issues with fewer assumptions, such as the incorporation of plate tectonics simulation with more realistic mantle rheology [51] or the use of 3D spherical geometry [52], both of which stretch the current computational techniques and resources. Nevertheless, we expect that the 2D cylindrical approximation will remain a useful tool, particularly for indicators that are in proportion to the modeled mantle volume, such as the percentage of degassing, ratio of heat and helium loss or isotopic ratios. Unless it can be demonstrated that the 3D geometry is essential for a certain proposed mechanism we would predict that the first order observables of mantle heterogeneity should be reproducible even in a simplified 2D model.

We are left with the conclusion that the geochemical constraints still demand a boundary layer or other form of mantle segregation, providing a radioelement-rich domain that releases heat in preference to helium. While most workers also assume that the primitive ^{3}He is also within this deep reservoir, other sources cannot at this stage be completely discounted [53]. The challenge re-

mains to identify the mechanism by which such a deep geochemical reservoir is preserved and has evolved, to incorporate this within numerical simulations of mantle dynamics, and reproduce first order observations of ^{3}He/^{4}He, radioelement distribution and heat/^{4}He.

6. Summary

Heat and He extraction in dynamical models show that there is a large degree of variance from the average heat/He due to the differential extraction of heat and He from the mantle system. Excursions from the model average value to the value observed in the Earth may be possible but would require a mantle with a noble gas concentration far higher than current estimates. The heat/He imbalance is a robust observation. Coupled with the requirement for a mantle domain with a high radioelement concentration to complement the depleted MORB-source mantle, there remains a convincing argument for a deep boundary layer in the mantle system.

Acknowledgements

We thank Geoff Davies, Mark Rehkämper and Alex Halliday for discussions. David Hilton and an anonymous reviewer are gratefully acknowledged for their constructive reviews. *[SK]*

References

[1] R.K. O'Nions, E.R. Oxburgh, Heat and helium in the Earth, Nature 306 (1983) 429–431.
[2] S.J.G. Galer, R.K. O'Nions, Residence time of thorium, uranium and lead in the mantle with implications for mantle convection, Nature 316 (1985) 778–782.
[3] L.H. Kellogg, G.J. Wasserburg, The role of plumes in mantle helium fluxes, Earth Planet. Sci. Lett. 99 (1990) 276–289.
[4] D. Porcelli, G.J. Wasserburg, Mass transfer of helium, neon, argon and xenon through a steady-state upper mantle, Geochim. Cosmochim. Acta 59 (1995) 4921–4937.
[5] D. Porcelli, G.J. Wasserburg, Mass transfer of xenon through a steady-state upper mantle, Geochim. Cosmochim. Acta 59 (1995) 1991–2007.
[6] R.D. van der Hilst, S. Widiyantoro, E.R. Engdahl, Evidence for deep mantle circulation from global tomography, Nature 386 (1997) 578–584.
[7] H. Bijwaard, W. Spakman, Tomographic evidence for a narrow whole mantle plume below Iceland, Earth Planet. Sci. Lett. 166 (1999) 121–126.
[8] P.E. van Keken, C.J. Ballentine, Whole mantle versus layered mantle convection and the role of a high-viscosity lower mantle in terrestrial volatile evolution, Earth Planet. Sci. Lett. 156 (1998) 19–32.
[9] P.E. van Keken, C.J. Ballentine, Dynamical models of mantle volatile evolution and the role of phase changes and temperature-dependent rheology, J. Geophys. Res. 104 (1999) 7137–7169.
[10] A. Rocholl, K.P. Jochum, Th, U and other trace elements in carbonaceous chondrites – implications for the terrestrial and solar system Th/U ratios, Earth Planet. Sci. Lett. 117 (1993) 265–278.
[11] B.R. Doe, R.E. Zartman, Plumbotectonics I, the Phanerozoic, in: H.L. Barnes (Ed.), Geochemistry of Hydrothermal Ore Deposits, Wiley, New York, 1979, pp. 22–70.
[12] K.P. Jochum, A.W. Hofmann, E. Ito, H.M. Seufert, W.M. White, K, U, and Th in mid-ocean ridge basalt glasses and heat production, K/U and K/Rb in the mantle, Nature 306 (1983) 431–436.
[13] W.R. Van Schmus, Natural radioactivity of the crust and mantle, in: T.J. Ahrens (Ed.), Global Earth Physics, A Handbook of Physical Constants, AGU Reference Shelf 1, American Geophysical Union, Washington, DC, 1995, pp. 283–291.
[14] F. Albarde, Time dependent models of U-Th-He and K-Ar evolution and the layering of mantle convection, Chem. Geol. 145 (1995) 413–429.
[15] S.R. Taylor, S.M. McClennan, The Continental Crust: Its Composition and Evolution, Blackwell, Cambridge, MA, 1985, 312 pp.
[16] R.L. Rudnick, D.M. Fountain, Nature and composition of the continental crust: a lower crustal perspective, Rev. Geophys. 33 (1995) 267–309.
[17] T. Torgersen, W.B. Clarke, Helium accumulation in groundwater. I. An evaluation of sources and the continental flux of crustal ^{4}Hein the Great Artesian Basin, Australia, Geochim. Cosmochim. Acta 49 (1985) 1211–1215.
[18] T. Torgersen, G.N. Ivey, Helium accumulation in groundwater. II. A model for the accumulation of the crustal ^{4}He degassing flux, Geochim. Cosmochim. Acta 49 (1985) 2445–2452.
[19] R.K. O'Nions, E.R. Oxburgh, Helium, volatile fluxes and the development of continental crust, Earth Planet. Sci. Lett. 90 (1988) 331–347.
[20] H.N. Pollack, S.J. Hurter, R. Johnston, Heat loss from the earth's interior: analysis of the global data set, Rev. Geophys. 31 (1993) 267–280.
[21] B.A. Buffett, H.E. Huppert, J.R. Lister, A.W. Woods, On the thermal evolution of the Earth's core, J. Geophys. Res. 101 (1996) 7989–8006.

[22] G.A. Glatzmaier, R.S. Coe, L. Hongre, P.H. Roberts, The role of the Earth's mantle in controlling the frequency of geomagnetic reversals, Nature 401 (1999) 885.
[23] D.A. Abbott, L. Burgess, J. Longhi, W.H.F. Smith, An empirical thermal history of the Earth's upper mantle, J. Geophys. Res. 99 (1994) 13835–13850.
[24] H. Craig, W.B. Clarke, M.A. Beg, Excess ^{3}He in deep water on the East Pacific Rise, Earth Planet. Sci. Lett. 26 (1975) 125–132.
[25] K.A. Farley, E. Maier-Reimer, P. Schlosser, W.S. Broecker, Constraints on mantle ^{3}He fluxes and deep-sea circulation from an oceanic general circulation model, J. Geophys. Res. 100 (1995) 3829–3839.
[26] A. Reymer, G. Schubert, Phanerozoic addition rates to the continental crust and crustal growth, Tectonics 3 (1984) 63–77.
[27] R.L. Armstrong, The persistent myth of crustal growth, Austral. J. Earth Sci. 38 (1991) 613–630.
[28] J.G. Schilling, C.K. Unni, M.L. Bender, Origin of chlorine and bromine in the oceans, Nature 273 (1978) 631–636.
[29] R. Batiza, Abundances, distribution and sizes of volcanos in the Pacific Ocean and implications for the origin of non-hotspot volcanos, Earth Planet. Sci. Lett. 60 (1982) 195–206.
[30] J.A. Crisp, Rates of magma emplacement and volcanic output, J. Volcanol. Geotherm. Res. 89 (1984) 3031–3049.
[31] B. Parsons, The rates of plate creation and consumption, Geophys. J. R. Astron. Soc. 67 (1981) 437–448.
[32] T. Torgersen, Terrestrial helium degassing fluxes and the atmospheric helium budget: implications with respect to the degassing processes of continental crust, Chem. Geol. 79 (1989) 1–14.
[33] D.R. Hilton, G.M. McMurtry, R. Kreulen, Evidence for extensive degassing of the Hawaiian mantle plume from helium-carbon relationships at Kilauea volcano, Geophys. Res. Lett. 24 (1997) 3065–3068.
[34] N.H. Sleep, Gradual entrainment of a chemical layer at the base of the mantle by overlying convection, Geophys. J. Int. 95 (1988) 437–447.
[35] G.T. Jarvis, D.P. McKenzie, Convection in a compressible fluid with infinite Prandtl number, J. Fluid Mech. 96 (1980) 515–583.
[36] V.I. Vangelov, G.T. Jarvis, Geometrical effects of curvature in axisymmetrical spherical models of mantle convection, J. Geophys. Res. 99 (1994) 9345–9358.
[37] P.E. van Keken, Cylindrical scaling for dynamical cooling models of the Earth, Phys. Earth Planet. Inter. 124 (2001) 119–130.
[38] P.E. van Keken, D.A. Yuen, A.P. van den Berg, Implications for mantle dynamics from the high melting temperature of perovskite, Science 264 (1994) 1437–1440.
[39] C. Cuvelier, A. Segal, A.A. Van Steenhoven, Finite Element Methods and the Navier–Stokes Equations, Reidel, Dordrecht, 1986.
[40] A.P. van den Berg, P.E. van Keken, D.A. Yuen, The effects of a composite non-Newtonian and Newtonian rheology on mantle convection, Geophys. J. Int. 115 (1993) 62–78.
[41] B. Blankenbach, F. Busse, U. Christensen, L. Cserepes, D. Gunkel, U. Hansen, H. Harder, G. Jarvis, M. Koch, G. Marquart, D. Moore, P. Olson, H. Schmeling, T. Schnaubelt, A benchmark comparison for mantle convection codes, Geophys. J. Int. 98 (1989) 23–38.
[42] P.E. van Keken, S.D. King, H. Schmeling, U.R. Christensen, D. Neumeister, M.P. Doin, A comparison of methods for the modeling of thermochemical convection, J. Geophys. Res. 102 (1997) 22,477–22,495.
[43] Y. Ricard, B. Wuming, Inferring the viscosity and 3-D density structure of the mantle from geoid, topography and plate velocities, Geophys. J. Int. 105 (1991) 561–571.
[44] D.R. Hilton, K. Hammerschmidt, G. Loock, H. Friedrichsen, Helium and argon isotope systematics of the central Lau Basin and Valu Fa Ridge: evidence of crust/mantle interactions in a back-arc basin, Geochim. Cosmochim. Acta 57 (1993) 2819–2841.
[45] A.W. Hofmann, Mantle geochemistry: the message from oceanic volcanism, Nature 385 (1997) 219–229.
[46] L.H. Kellogg, B.H. Hager, R.D. van der Hilst, Compositional stratification in the deep mantle, Science 283 (1999) 1881–1884.
[47] A.K. McNamara, P.E. van Keken, Cooling of the Earth: a parameterized convection study of whole vs. layered models, Geochem. Geophys. Geosyst. 1 (2000).
[48] P.J. Tackley, Three-dimensional simulations of mantle convection with a thermo-chemical basal boundary layer: D″?, in: M. Gurnis, M.E. Wysession, E. Knittle, B.A. Buffett (Eds.), The Core-Mantle Boundary Region, Geodynamics Series, Vol. 28, American Geophysical Union, Washington, DC, 1998, pp. 231–254.
[49] T.W. Becker, J.B. Kellogg, R.J. O'Connell, Thermal constraints on the survival of primitive blobs in the lower mantle, Earth Planet. Sci. Lett. 171 (1999) 351–365.
[50] N. Coltice, Y. Ricard, Geochemical observations and one layer mantle convection, Earth Planet. Sci. Lett. 174 (1999) 125–137.
[51] P.J. Tackley, Mantle convection and plate tectonics toward an integrated physical and chemical theory, Science 288 (2000) 2002–2007.
[52] P.E. van Keken, S.J. Zhong, Mixing in a 3D spherical model of present day mantle convection, Earth Planet. Sci. Lett. 171 (1999) 533–547.
[53] D. Porcelli, A.N. Halliday, The possibility of the core as a source of mantle helium, Earth Planet. Sci. Lett. (2000) submitted.